Gaussian packet prestack depth migration

Karel Žáček
Department of Geophysics, Faculty of Mathematics and Physics, Charles University, Ke Karlovu 3, 121 16 Praha 2, Czech Republic, E-mail: zacek@karel.troja.mff.cuni.cz

Summary

We present a complete algorithm and the first complete 2-D acoustic numerical examples of a brand new imaging method operating in the common-shot domain — the Gaussian packet prestack depth migration.

The main advantage of our method over the methods based on Gaussian beams is a direct relation between the regions in the common-shot gather and corresponding regions in the migrated section. Thus, the Gaussian packet prestack depth migration is especially suitable for a target-oriented imaging.

Key words

Gaussian packet, Gabor function, prestack depth migration, target-oriented imaging, multi-valued travel time, common-shot gather.

1 Introduction

Over the past years, several imaging techniques based on the seismic ray theory have been developed. Particularly simple and popular are the methods using the Kirchhoff integral. Another successful class of ray theory migrations employs Gaussian beams. An especially elegant and effective migration algorithm using Gaussian beams has been proposed by Hill (1990, 2001).

In search for an alternative to Gaussian beams, we have shifted our attention to Gaussian packets. Gaussian packets are waves whose envelopes at any given time are nearly Gaussian in space. They represent high-frequency asymptotic solutions of the elastodynamic equation, which are concentrated close to the central point of the packet (e.g., Babich & Ulin, 1981; Ralston, 1983; Klimeš, 1989a, 2004).

Like Gaussian beams, Gaussian packets become inaccurate solutions of the elastodynamic equation if they spread excessively as they propagate. This spreading depends on the complexity of the velocity model and on the initial shape of Gaussian packets. Thus, we should use a sufficiently smooth velocity model and optimize the initial shape of the packets.

The Gaussian packet migration algorithm consists of four basic steps:
a) Preparation of a suitable smooth velocity model (Žáček, 2002).
b) Optimization of the shape of Gaussian packets (Klimeš, 1989b; Žáček, 2001a, 2001b).
c) Decomposition of the wave field into optimized Gaussian packets (Žáček, 2003, 2005).
d) Back-propagation of the wave field using Gaussian packets and application of the imaging functional, which was already presented by Žáček (2004), and which we thoroughly describe in this paper.

The word *optimized* implies that the shape of Gaussian packets, in the plane perpendicular to the central ray of the packet, depends not only on the frequency, but

In: Seismic Waves in Complex 3-D Structures, Report 15 (Department of Geophysics, Charles University, Prague, 2005), pp.29–48

also on the coordinate of the intersection of the central ray of a Gaussian packet with the profile, on its arrival time, and on the component of the slowness vector along the profile.

The migration algorithm is designed here especially for numerical testing in the 2-D acoustic Marmousi model (Versteeg & Grau, 1991). That is why only scalar waves are dealt with in the imaging part of this paper, although the generalization of the Gaussian packet migration to the elastic waves is straightforward.

2 Paraxial Gaussian packet

In the case of the component notation, the upper-case indices take the values $I, J, ... = 1, 2$; the lower-case indices take the values $i, j, ... = 1, 2, 3$; the Greek indices take the values $\alpha, \beta, ... = 1, 2, 3, 4$. The Einstein summation over the pairs of identical indices is used. The asterisk (e.g., u^*) denotes the complex conjugate.

Let us write the space-time paraxial approximation of a Gaussian packet centred at point $y_\alpha(t)$ in the form of

$$\mathbf{U} = \mathbf{A} \exp\left[\mathrm{i}\omega(N_\alpha r_\alpha + \tfrac{1}{2} N_{\alpha\beta} r_\alpha r_\beta)\right] \quad , \tag{1}$$

where

$$r_i = x_i - y_i(t) \quad , \tag{2}$$

$$r_4 = x_4 - y_4(t) = x_4 - t \quad , \tag{3}$$

$$N_{\alpha\beta} = \tau_{,\alpha\beta} \tag{4}$$

and

$$N_\alpha = \tau_{,\alpha} \quad . \tag{5}$$

Here, τ denotes the complex-valued phase function. The complex-valued vectorial amplitude $\mathbf{A}$, the complex-valued second space-time derivatives of the phase function $N_{\alpha\beta}$ and the space-time slowness vector of the Gaussian packet N_α are taken at the central point $y_\alpha(t)$ of the packet. We choose

$$N_4 = -1 \quad . \tag{6}$$

As it is much easier to deal with Gaussian packets in the *ray-centred coordinate system* (e.g., Červený, 2001), we constitute the transform relations between the Cartesian and ray-centred coordinates. In our notation, h_{im} represents the i^{th} component of m^{th} orthonormal basis vector of the ray-centred coordinate system. Basis vectors h_{i1} and h_{i2} are perpendicular to the central ray; basis vector h_{i3} is tangent to the central ray.

The complex-valued second covariant derivatives $M_{\alpha\beta}$ of the phase function in ray-centred coordinates are related to the second space-time derivatives $N_{\alpha\beta}$ of the phase function in Cartesian coordinates as

$$M_{mn} = N_{jk} h_{jm} h_{kn} \quad , \tag{7}$$

$$N_{jk} = h_{jm} h_{kn} M_{mn} \quad , \tag{8}$$

$$M_{m4} = M_{4m} = N_{j4} h_{jm} \quad , \tag{9}$$

$$N_{j4} = N_{4j} = h_{jm} M_{m4} \tag{10}$$

and

$$M_{44} = N_{44} \quad . \tag{11}$$

Differentiating the eikonal equation

$$v^2\tau_{,i}\tau_{,i} - \tau_{,4}\tau_{,4} = 0 \tag{12}$$

with respect to space-time coordinates, and using relation (6), we arrive at

$$M_{i4} = -vM_{i3} - v^{-1}V_i \tag{13}$$

and

$$M_{44} = v^2 M_{33} + V_3 \quad , \tag{14}$$

where

$$V_m = v_{,i}h_{im} \tag{15}$$

is the velocity gradient in ray-centred coordinates.

Differentiating twice the eikonal equation (12) with respect to space-time coordinates, we obtain the Ricatti equation for the 4×4 space-time matrix (4), see Ralston (1983). Using relations (7) to (11), let us transform the Ricatti equation into the ray-centred coordinate system. Inserting equations (13) and (14), we obtain the Ricatti equation for the 3×3 spatial submatrix M_{mn} of the 4×4 space-time matrix $M_{\alpha\beta}$,

$$\frac{\mathrm{d}M_{mn}}{\mathrm{d}t} = -M_{jn}\frac{\mathrm{d}h_{ij}}{\mathrm{d}t}h_{im} - M_{mk}\frac{\mathrm{d}h_{ik}}{\mathrm{d}t}h_{in} - v^2 M_{Km}M_{Kn} - v^{-1}V_{mn} - V_m M_{3n} - V_n M_{3m} \quad , \tag{16}$$

where

$$V_{mn} = v_{,ij}h_{im}h_{jn} \tag{17}$$

are the covariant velocity derivatives in ray-centred coordinates. The derivatives of the basis vectors of the ray-centred coordinate system along the ray satisfy relations

$$\frac{\mathrm{d}h_{jM}}{\mathrm{d}t}h_{jN} = 0 \; , \quad \frac{\mathrm{d}h_{j3}}{\mathrm{d}t}h_{jN} = -V_N \; , \quad \frac{\mathrm{d}h_{jM}}{\mathrm{d}t}h_{j3} = V_M \; , \quad \frac{\mathrm{d}h_{j3}}{\mathrm{d}t}h_{j3} = 0 \quad . \tag{18}$$

Inserting relations (18), equation (16) may be decoupled into three equations,

$$\frac{\mathrm{d}M_{MN}}{\mathrm{d}t} = -v^2 M_{MK}M_{KN} - v^{-1}V_{MN} \quad , \tag{19}$$

$$\frac{\mathrm{d}M_{M3}}{\mathrm{d}t} = -M_{Mi}V_i - v^2 M_{MI}M_{I3} - v^{-1}V_{M3} \tag{20}$$

and

$$\frac{\mathrm{d}M_{33}}{\mathrm{d}t} = -2M_{i3}V_i - v^2 M_{3I}M_{I3} - v^{-1}V_{33} \quad . \tag{21}$$

While equation (19) is the Ricatti equation for a Gaussian beam, equations (20) and (21) extend the Gaussian beam solution to a Gaussian packet solution.

To express equations (19), (20) and (21) in the vector and matrix notation, we introduce following matrices and vectors,

$$\mathbf{M} = \begin{pmatrix} M_{11} & M_{12} \\ M_{21} & M_{22} \end{pmatrix} \quad , \tag{22}$$

$$\mathbf{M}_3 = \begin{pmatrix} M_{13} \\ M_{23} \end{pmatrix} \quad , \tag{23}$$

$$\mathbf{M}_4 = \begin{pmatrix} M_{14} \\ M_{24} \end{pmatrix} \quad , \tag{24}$$

$$\mathbf{W} = \begin{pmatrix} V_{11} & V_{12} \\ V_{21} & V_{22} \end{pmatrix} \tag{25}$$

and

$$\mathbf{V} = \begin{pmatrix} V_1 \\ V_2 \end{pmatrix} \quad . \tag{26}$$

The Ricatti equation for a Gaussian beam (19) in the matrix notation reads

$$\frac{\mathrm{d}\mathbf{M}}{\mathrm{d}t} = -v^2\mathbf{M}\mathbf{M} - v^{-1}\mathbf{W} \quad . \tag{27}$$

Its solution may be expressed as

$$\mathbf{M} = \mathbf{M}^{\mathrm{T}} = \mathbf{P}\mathbf{Q}^{-1} \quad , \tag{28}$$

where matrices $\mathbf{Q}$ and $\mathbf{P}$ satisfy the dynamic ray tracing equations (e.g., Červený, 2001)

$$\frac{\mathrm{d}\mathbf{Q}}{\mathrm{d}t} = v^2\mathbf{P} \quad , \qquad \frac{\mathrm{d}\mathbf{P}}{\mathrm{d}t} = -v^{-1}\mathbf{W}\mathbf{Q} \quad . \tag{29}$$

We introduce the *paraxial-ray propagator matrix*

$$\mathbf{\Pi} = \begin{pmatrix} \mathbf{Q}_1 & \mathbf{Q}_2 \\ \mathbf{P}_1 & \mathbf{P}_2 \end{pmatrix} \quad , \tag{30}$$

which solves equations (29) with unit initial conditions

$$\begin{pmatrix} \mathbf{Q}_1^0 & \mathbf{Q}_2^0 \\ \mathbf{P}_1^0 & \mathbf{P}_2^0 \end{pmatrix} = \begin{pmatrix} \mathbf{1} & \mathbf{0} \\ \mathbf{0} & \mathbf{1} \end{pmatrix} \quad , \tag{31}$$

where $\mathbf{1}$ denotes a unit 2×2 matrix. Matrices $\mathbf{Q}$ and $\mathbf{P}$ may be determined from their initial values $\mathbf{Q}^0$ and $\mathbf{P}^0$ using the paraxial-ray propagator matrix as

$$\begin{pmatrix} \mathbf{Q} \\ \mathbf{P} \end{pmatrix} = \mathbf{\Pi} \begin{pmatrix} \mathbf{Q}^0 \\ \mathbf{P}^0 \end{pmatrix} \quad . \tag{32}$$

Equations (20) and (21), which extend the Gaussian beam solution of the Ricatti equation to a Gaussian packet solution, may be rewritten in the vector and matrix notation as follows,

$$\frac{\mathrm{d}(v\mathbf{M}_3 + v^{-1}\mathbf{V})}{\mathrm{d}t} = -v^2\mathbf{M}(v\mathbf{M}_3 + v^{-1}\mathbf{V}) \tag{33}$$

and

$$\frac{\mathrm{d}M_{33}}{\mathrm{d}t} = -2V_3M_{33} - v^2(\mathbf{M}_3 + v^{-2}\mathbf{V})^{\mathrm{T}}(\mathbf{M}_3 + v^{-2}\mathbf{V}) + v^{-2}\mathbf{V}^{\mathrm{T}}\mathbf{V} - v^{-1}V_{33} \quad . \tag{34}$$

Solutions of equations (33) and (34) read

$$\mathbf{M}_3 = v^{-1}\left[(\mathbf{Q}^{\mathrm{T}})^{-1}\mathbf{C} - v^{-1}\mathbf{V}\right] \tag{35}$$

and

$$M_{33} = v^{-2}\left\{-\frac{\mathrm{i}}{2}\mathbf{C}^{\mathrm{T}}\mathbf{Q}^{-1}\left[\mathrm{Im}(\mathbf{M})\right]^{-1}(\mathbf{Q}^{\mathrm{T}})^{-1}\mathbf{C} + C - V_3\right\} \quad , \tag{36}$$

where $\mathbf{C}$ is a constant vector determined by the initial conditions and C is an integration constant. Equations for elements $\mathbf{M}_3$, $\mathbf{M}_4$, M_{33}, M_{34} and M_{44}, which supplement the 2×2 Gaussian beam matrix M_{MN} to the 4×4 Gaussian packet matrix $M_{\alpha\beta}$, consist of two explicit evolution equations,

$$\mathbf{M}_4 = -(\mathbf{Q}^{\mathrm{T}})^{-1}\mathbf{C} \tag{37}$$

(Babich & Ulin, 1981),

$$M_{44} = -\frac{\mathrm{i}}{2}\mathbf{C}^{\mathrm{T}}\mathbf{Q}^{-1}\left[\mathrm{Im}(\mathbf{M})\right]^{-1}(\mathbf{Q}^{\mathrm{T}})^{-1}\mathbf{C} + C = -\frac{\mathrm{i}}{2}\mathbf{M}_4^{\mathrm{T}}\left[\mathrm{Im}(\mathbf{M})\right]^{-1}\mathbf{M}_4 + C \quad , \tag{38}$$

and three simple relations,

$$\mathbf{M}_3 = -v^{-1}\mathbf{M}_4 - v^{-2}\mathbf{V} \quad , \tag{39}$$

$$M_{33} = v^{-2}\left(M_{44} - V_3\right) \tag{40}$$

and

$$M_{34} = -v^{-1}M_{44} \quad . \tag{41}$$

Following equations (37) and (38), we determine constants $\mathbf{C}$ and C from the initial values $\mathbf{M}_4^0$ and M_{44}^0 of elements $\mathbf{M}_4$ and M_{44},

$$\mathbf{C} = -\mathbf{Q}^{0\,\mathrm{T}}\mathbf{M}_4^0 \tag{42}$$

and

$$C = M_{44}^0 + \frac{\mathrm{i}}{2}\mathbf{M}_4^{0\,\mathrm{T}}\left[\mathrm{Im}(\mathbf{M}^0)\right]^{-1}\mathbf{M}_4^0 \quad . \tag{43}$$

The complex-valued vectorial amplitude of a Gaussian packet $\mathbf{A}$, see equation (1), may be expressed as

$$\mathbf{A} = A\mathbf{e} \quad , \tag{44}$$

where A is the complex-valued scalar amplitude; $\mathbf{e}$ denotes the unit polarization vector of a Gaussian packet, which is identical to the Gaussian beam polarization vector and to the ray-theory polarization vector. The complex-valued scalar amplitude evolves along the central ray of a Gaussian packet according to equation (Babich & Ulin, 1981)

$$A = A^0\sqrt{\frac{v^0\rho^0\det(\mathbf{Q}^0)}{v\rho\,\det(\mathbf{Q})}} \quad , \tag{45}$$

where velocity v and density ρ correspond to the elastodynamic equation and should be replaced by respective material parameters for other wave equations.

3 Imaging

We choose the imaging functional for scalar waves in the form of

$$M(u,U) = \int\mathrm{d}\omega\;\frac{\widehat{F}(\omega)\widehat{u}^*(\omega)\widehat{U}(\omega)}{\widehat{u}^*(\omega)\widehat{u}(\omega)}\left[\int\mathrm{d}\omega\;\widehat{F}(\omega)\right]^{-1} \quad , \tag{46}$$

where $\widehat{u}$ is the temporal Fourier transform of the incident wavefield u and $\widehat{U}$ is the temporal Fourier transform of the back-propagated scattered wavefield U. Let us take the spectral filter $\widehat{F}$ in the form of the Fourier transform $\widehat{s}$ of the source time function s, possibly shifted by time $-t_{\mathrm{S}}$ or phase $-\varphi_{\mathrm{S}}$,

$$\widehat{F}(\omega) = \widehat{s}(\omega)\exp(\mathrm{i}\varphi_{\mathrm{S}} - \mathrm{i}\omega t_{\mathrm{S}}) \quad . \tag{47}$$

We assume the incident wavefield $\widehat{u}(\omega)$ approximated by several ray-theory elementary seismograms $\widehat{u}_\Omega(\omega)$ corresponding to individual branches Ω of possibly multi-valued travel time,

$$\widehat{u}(\omega) = \sum_\Omega \widehat{u}_\Omega(\omega) \quad , \tag{48}$$

with

$$\widehat{u}_{\Omega}(\omega) = \widehat{s}(\omega)\widehat{a}_{\Omega}\exp(\mathrm{i}\omega\tau_{\Omega}) \quad , \tag{49}$$

where a_{Ω} is the amplitude corresponding to travel time τ_{Ω}. To avoid singularities and to simplify the calculation, we apply approximation

$$\widehat{u}^*(\omega)\widehat{u}(\omega) \approx \widehat{s}^*(\omega)\widehat{s}(\omega)\sum_{\Omega}\widehat{a}^*_{\Omega}(\omega)\widehat{a}_{\Omega}(\omega) \quad . \tag{50}$$

The back-propagated scattered wavefield may be composed of individual Gaussian packets U_{R},

$$\widehat{U}(\omega) = \sum_{\mathrm{R}}\widehat{U}_{\mathrm{R}}(\omega) \quad . \tag{51}$$

Then, the imaging functional takes the form of

$$M(u,U) = \sum_{\mathrm{R}} M(u,U_{\mathrm{R}}) \quad , \tag{52}$$

where

$$M(u,U_{\mathrm{R}}) \approx \int\!\mathrm{d}\omega\ \frac{\exp(\mathrm{i}\varphi_{\mathrm{S}} - \mathrm{i}\omega t_{\mathrm{S}})\sum_{\Omega}\widehat{a}^*_{\Omega}(\omega)\exp(-\mathrm{i}\omega\tau_{\Omega})\,\widehat{U}_{\mathrm{R}}(\omega)}{\sum_{\Omega}\widehat{a}^*_{\Omega}(\omega)\widehat{a}_{\Omega}(\omega)}\ \left[\int\!\mathrm{d}\omega\ \widehat{F}(\omega)\right]^{-1} . \tag{53}$$

In the time domain, equation (53) reads

$$M(u,U_{\mathrm{R}}) \approx \frac{\sum_{\Omega}\exp(\mathrm{i}\varphi_{\mathrm{S}})\,a^*_{\Omega}\,U_{\mathrm{R}}(t_{\mathrm{S}}+\tau_{\Omega})}{F(0)\ \sum_{\Omega}a^*_{\Omega}a_{\Omega}} \quad . \tag{54}$$

Although Gaussian packets are moving from the target zone towards the corresponding receiver, we expect that the central rays of the packets are calculated from the receiver towards the target zone.

Travel time T from the receiver is then used as the parameter along the central ray, whereas $y_i(T)$ and $y_4(T) = t_{\mathrm{R}} - T$ are spatial coordinates and the travel time corresponding to the centre of the Gaussian packet moving towards the receiver, respectively.

Because of the opposite propagation, the slowness vector of the packet N_i is minus the slowness vector P_i of the ray coming from the receiver,

$$N_i = -P_i \quad . \tag{55}$$

We choose

$$N_4 = -1 \quad . \tag{56}$$

Paraxial approximation of a Gaussian packet propagating towards the corresponding receiver to reach it at time $x_4 = t_{\mathrm{R}}$, centred at point $y_{\alpha}(T)$, is

$$U_{\mathrm{RT}}(x_4) = A_{\mathrm{RT}}\exp\left[\mathrm{i}\omega(N_{\alpha}r_{\alpha} + \tfrac{1}{2}N_{\alpha\beta}r_{\alpha}r_{\beta})\right] \quad , \tag{57}$$

where

$$r_i = x_i - y_i(T) \tag{58}$$

and

$$r_4 = x_4 - y_4(T) = x_4 - (t_{\mathrm{R}} - T) \quad . \tag{59}$$

Matrix $N_{\alpha\beta}$ corresponds to a Gaussian packet moving towards a receiver, although it is, like the travel time y_4 and slowness vector N_{α}, expressed in terms of the quantities calculated along the ray emanated from the receiver.

Paraxial approximation (57) is accurate in the vicinity of point $y_\alpha(T)$, but becomes inaccurate at large space-time distances from $y_\alpha(T)$. Assuming discrete points $y_i(T)$ with step ΔT along the central ray, we thus limit each paraxial approximation by weighting function

$$W_{\mathrm{T}} = \sqrt{\pi}\,\kappa^{-1}\,\exp\left[-\kappa^2(N_i r_i)^2 \Delta T^{-2}\right] \quad , \tag{60}$$

where parameter κ controls the shape of the Gaussian function and, consequently, the error of the weighting. Sum of these weighting functions is approximately 1 in the vicinity of the central ray and thus

$$U_{\mathrm{R}}(t_{\mathrm{S}} + \tau_\Omega) = \sum_{\mathrm{T}} W_{\mathrm{T}}\, U_{\mathrm{RT}}(t_{\mathrm{S}} + \tau_\Omega) \quad . \tag{61}$$

According to equations (54) and (61), the image of a single Gaussian packet reads

$$M(u, U_{\mathrm{R}}) = \sum_{\mathrm{T}} M(u, W_{\mathrm{T}} U_{\mathrm{RT}}) \quad , \tag{62}$$

where the image of a single paraxial approximation is

$$M(u, W_{\mathrm{T}} U_{\mathrm{RT}}) = \frac{\sqrt{\pi}\sum_\Omega a_\Omega^*\, A_{\mathrm{RT}}\ \exp\left[\mathrm{i}\varphi_{\mathrm{S}} + \mathrm{i}\omega(N_\alpha r_\alpha + \frac{1}{2}N_{\alpha\beta} r_\alpha r_\beta) - \kappa^2 (N_i r_i)^2 \Delta T^{-2}\right]}{F(0)\ \kappa\ \sum_\Omega a_\Omega^* a_\Omega} \ , \tag{63}$$

with

$$r_4 = t_{\mathrm{S}} + \tau_\Omega(x_i) + T - t_{\mathrm{R}} \quad . \tag{64}$$

Inserting equation (62) into (52), the imaging functional takes the form of

$$M(u, U) = \sum_{\mathrm{R}} \sum_{\mathrm{T}} M(u, W_{\mathrm{T}} U_{\mathrm{RT}}) \quad . \tag{65}$$

4 Algorithm

Like other types of wave packets, Gaussian packets spread as they propagate through the structure. It is necessary to keep Gaussian packets narrow in relation to the velocity changes in the model, because Gaussian packets become inaccurate solutions of the elastodynamic equation if the velocity field changes considerably within the packet width. This spreading depends on the complexity of the velocity model and on the initial shape of Gaussian packets. Therefore, before proceeding to the migration, we need to prepare a suitable velocity model and choose the appropriate initial shape of Gaussian packets.

Since the Gaussian packet prestack depth migration operates in the wave field domain, the initial amplitudes of Gaussian packets are obtained by decomposing the common-shot gathers into Gabor functions.

In the process of imaging, we compare the incident wave field u and the back-propagated scattered wave field U. The back-propagated wave field consists of individual Gaussian packets. We choose the imaging functional in the form of expression (46), although other varieties of imaging functionals could be admissible as well.

4.1 Velocity model

A velocity model should prevent Gaussian packets from excessive spreading and approximately preserve original travel times. The question of the smoothness of the velocity model is closely related to the problem of finding the limits of applicability of the ray theory, which remains unsolved and open for further research.

In a complex model, the geometrical spreading and number of arrivals exponentially increase with increasing travel time. The exponential increment is controlled by the Lyapunov exponent (e.g., Klimeš, 2002). Consequently, the Lyapunov exponent determines the horizon, where the ray behavior becomes chaotic. Since the Lyapunov exponent depends on the second spatial derivatives of the velocity or slowness, the second derivatives should be minimized. Therefore, we smooth the second derivatives of slowness by minimizing the relevant Sobolev norm (Žáček, 2002).

4.2 Optimization of the shape of Gaussian packets

The applicability and accuracy of the Gaussian packet method depend on the proper choice of the initial shape of packets. Unfortunately, narrow Gaussian packets quickly increase in width as they propagate. Thus, we can use neither too narrow nor too wide packets as the initial choice of the shape of Gaussian packets. Furthermore, in a complex structure, we cannot judge solely from the final width of the packet whether the packet is or is not a reasonably accurate solution of the elastodynamic equation. The packet must be sufficiently narrow along the whole ray path.

The initial shape of Gaussian packets is determined by the complex-valued second space-time derivatives of the phase function $N^0_{\alpha\beta}$, see equation (1). To prevent Gaussian packets from excessive spreading, we optimize their initial shape by minimizing their width along the whole ray path. Since we wish to control the spreading in the plane perpendicular to the central ray of the packet, see equation (27), it is sufficient to optimize the initial shape of corresponding Gaussian beams (Klimeš, 1989b; Žáček, 2001a, 2001b). We can restrict our attention to Gaussian beams, because the Ricatti equation for a Gaussian packet (16) may be decoupled into three equations, where equation (19) is the Ricatti equation for a Gaussian beam, and equations (20) and (21) extend the Gaussian beam solution to a Gaussian packet solution.

The shape of a Gaussian beam is characterized by a 2×2 complex-valued matrix in 3-D and by a single complex number in 2-D. Let us denote by N^0 the initial complex-valued parameter in 2-D, which was defined as parameter N by Žáček (2005). The imaginary part of N^0 determines the Gaussian beam width and the real part of N^0 defines the curvature of the phase-front.

Parameter N^0, which describes the shape of a corresponding Gaussian beam along the initial surface, may depend on the coordinate of the intersection of the central ray of a Gaussian packet with the profile x_{R}, on its arrival time t_{R}, and on the component of the slowness vector along the profile p. In other words, parameter N^0 is situated on a *Hamiltonian hypersurface* in the phase-space (Žáček, 2001a, 2001b). In a complex structure, the optimum initial parameters $N^0(x_{\mathrm{R}}, t_{\mathrm{R}}, p)$ may vary in orders of magnitude. This would cause great problems in the decomposition of the wave field into optimized Gaussian packets. Therefore, we have developed a procedure, which allows us to smooth iteratively the distribution of parameter N^0 on the Hamiltonian hypersurface (Žáček, 2001a, 2001b).

4.3 Decomposition of the wave field into Gaussian packets

In order to determine the initial amplitudes of Gaussian packets A^0, see equation (45), we need to decompose the common-shot gather into optimized Gaussian packets (Žáček, 2003, 2005). Each Gaussian packet arriving at the receivers is represented by a Gabor function, whose shape depends on the shape of the Gaussian packet. Using the *coherent-state transform*, we decompose the common-shot gather into these Gabor functions. The complex valued amplitude of the back-propagated Gaussian packet A^0 then equals the amplitude of the corresponding Gabor function. The amplitudes depend on the coordinate of the intersection of the central ray of a Gaussian packet with the profile x_{R}, its arrival time t_{R}, the component of the slowness vector along the profile p, and the frequency ω. Let us point out that the intersection of the central ray of a Gaussian packet with the profile x_{R} does not generally coincide with any receiver.

In 2-D, the initial shape of a Gaussian packet is defined by two free complex-valued parameters — N^0 and K^0. Parameter N^0 should be determined by the optimization of the shape of corresponding Gaussian beams. We choose parameter K^0, which was introduced as parameter K_0 by Žáček (2005), and which describes the shape of a Gaussian packet along the central ray, pure imaginary and uniform for all Gaussian packets. Please note that parameter K^0 is used in the choice of N_{44}, see Žáček (2005, eq. 25) and equation (66) below.

Let us mention two problems closely connected with optimized Gaussian packets. The decomposition is exact only for N^0 independent on x_{R} and t_{R}. However, we may achieve satisfactory results for a reasonably smooth distribution of parameter N^0 on the Hamiltonian hypersurface (Žáček, 2003, 2005).

Unfortunately, the non-uniform shapes of Gaussian packets also affect the amount of data we have to work with, because the maximum steps in x_{R} and p depend on parameter N^0. In 2-D, for the imaginary part of N^0 varying from $[\mathrm{Im}(N^0)]_{\mathrm{MIN}}$ to $[\mathrm{Im}(N^0)]_{\mathrm{MAX}}$, the number of grid points in our 4-dimensional phase-space is approximately proportional to $\{[\mathrm{Im}(N^0)]_{\mathrm{MAX}}/[\mathrm{Im}(N^0)]_{\mathrm{MIN}}\}^{1/2}$. This could seriously jeopardize the efficiency of our method.

We overcome these difficulties by smoothing the distribution of parameter N^0 on the Hamiltonian hypersurface. To simplify the calculation, we can smooth N^0 to a constant value and obtain uniform Gaussian packets. Naturally, the smoothing brings about more rapid spreading of Gaussian packets.

4.4 Migration

We begin the main process of migration by determining the incident wave field u and the back-propagated scattered wave field U. Then, we construct the migrated image, which is given by expressions (63) and (65).

The incident wave field u may be calculated in various ways. We benefit from a method of interpolation within ray cells proposed by Bulant & Klimeš (1999), which requires only a sufficiently dense set of rays from the shot location to be traced. By interpolation, we obtain the multi-valued amplitudes of the incident wave field a_Ω corresponding to travel times τ_Ω.

We determine the scattered wave field U using the Gaussian packet method. Gaussian packets propagate along their central rays, which have to be shot with the same steps in x_{R} and p as in the decomposition of the wave field. We move along these central rays with step ΔT, determine matrix $N_{\alpha\beta}$ and the amplitude of a Gaussian packet A_{RT}, and calculate expression (63).

In 2-D, we choose basis vector h_{i1} perpendicular to the plane of calculation and, consequently, basis vector h_{i2} parallel to the plane of calculation. We select the Cartesian coordinate system with vector $(0,1,0)$ tangent to the initial surface in the plane of calculation and vector $(0,0,1)$ perpendicular to the initial surface. Then, matrix $M^0_{\alpha\beta}$ reads

$$\mathbf{M}^0 = \begin{pmatrix} 0 & 0 & 0 & 0 \\ 0 & \frac{N^0}{h_{22}^2} + 2\frac{V_2}{v^2}\frac{h_{23}}{h_{22}} + \frac{V_3}{v^2}\left(\frac{h_{23}}{h_{22}}\right)^2 & -\frac{V_2}{v^2} & 0 \\ 0 & -\frac{V_2}{v^2} & \frac{N^0_{44}-V_3}{v^2} & -\frac{N^0_{44}}{v} \\ 0 & 0 & -\frac{N^0_{44}}{v} & N^0_{44} \end{pmatrix} \quad , \tag{65}$$

see equations (8), (39) with $\mathbf{M}_4 = \mathbf{0}$, (40) and (41). Please note that parameter N^0 corresponds to N^0_{22}, see equation (8). According to Žáček (2005, eq. 31), we choose

$$N^0_{44}(x_{\mathrm{R}}, t_{\mathrm{R}}, p, \omega) = \frac{N^0(x_{\mathrm{R}}, t_{\mathrm{R}}, p)K^0}{\omega N^0(x_{\mathrm{R}}, t_{\mathrm{R}}, p) - p^2 K^0} \quad . \tag{66}$$

In order to calculate expressions (28), (37), (38), (39), (40) and (41), which yield matrix $M_{\alpha\beta}$ corresponding to its initial choice $M^0_{\alpha\beta}$, we need to determine matrices $\mathbf{Q}$ and $\mathbf{P}$. Since the central ray of a Gaussian packet is calculated from the surface towards the target zone, whereas the packet propagates from the target zone towards the surface, we have to change the sign of the slowness vector, see equation (55), and modify equation (32) into

$$\begin{pmatrix} \mathbf{Q} \\ \mathbf{P} \end{pmatrix} = \begin{pmatrix} \mathbf{Q}_1 & -\mathbf{Q}_2 \\ -\mathbf{P}_1 & \mathbf{P}_2 \end{pmatrix} \begin{pmatrix} \mathbf{Q}^0 \\ \mathbf{P}^0 \end{pmatrix} \quad , \tag{67}$$

where

$$\mathbf{Q}^0 = \begin{pmatrix} 1 & 0 \\ 0 & 1 \end{pmatrix} \tag{68}$$

and

$$\mathbf{P}^0 = \begin{pmatrix} 0 & 0 \\ 0 & M^0_{22} \end{pmatrix} \quad . \tag{69}$$

Using relations (8), (10) and (11), we transform matrix $M_{\alpha\beta}$ into matrix $N_{\alpha\beta}$, which describes the shape of a Gaussian packet in Cartesian coordinates.

The amplitude of a Gaussian packet evolves along the central ray according to equation (45). Following our choice of matrix $\mathbf{Q}^0$, see relation (68), we can write

$$A_{\mathrm{RT}} = A^0(x_{\mathrm{R}}, t_{\mathrm{R}}, p, \omega)\sqrt{\frac{v^0\rho^0}{v\rho}}\frac{1}{\sqrt{\det(\mathbf{Q})}} \quad , \tag{70}$$

where the initial amplitude A^0 comes from the decomposition of the wave field. In the case of forward propagation, the complex-valued square root depends on the number of caustic points along the central ray as

$$\frac{1}{\sqrt{\det(\mathbf{Q})}} = \sqrt{\frac{\mathrm{i}\ \mathrm{sgn}\left[\det(\mathbf{Q}_2)\right]}{\det(\mathbf{Q})}}\ \exp\left[-\mathrm{i}\frac{\pi}{4}(2k+1)\right] \quad , \tag{71}$$

where the square root is taken with the positive real part. Index k denotes the *KMAH* index, which is defined as the sum of the caustic points along the ray (e.g., Červený, 2001). As the Gaussian packet propagates from the target zone towards the surface, whereas the initial value of matrix $\mathbf{Q}$ is defined on the surface, we have to change the sign of the *KMAH* index. Thus,

$$A_{\mathrm{RT}} = A^0(x_{\mathrm{R}}, t_{\mathrm{R}}, p, \omega)\sqrt{\frac{v^0\rho^0}{v\rho}}\sqrt{\frac{\mathrm{i}\ \mathrm{sgn}\left[\det(\mathbf{Q}_2)\right]}{\det(\mathbf{Q})}}\ \exp\left[\mathrm{i}\frac{\pi}{4}(2k-1)\right] \quad . \tag{72}$$

As soon as we determine the multi-valued amplitudes of the incident wave field a_Ω corresponding to travel times τ_Ω, and the amplitude A_{RT} and the second space-time derivatives of the phase function $N_{\alpha\beta}$ of the back-propagated Gaussian packet, we calculate expression (62), which yields the localized image of a single Gabor function from the common-shot gather. Then, we superimpose the images of all Gabor functions corresponding to a single common-shot gather, see expression (65), and obtain the prestack migrated image of this common-shot gather. Finally, we can stack all of the images to produce the migrated image of the whole data set.

5 Target-oriented imaging

Each Gabor function from the common-shot gather generates its localized image in the depth section. In this way, we obtain a one-to-one relation between the Gabor functions from the common-shot gather and their localized images from the depth section. This relation was discussed in greater detail by Žáček & Klimeš (2003).

Let us say that we are interested in a particular area in the subsurface structure. We call this area a *target zone*. Unlike Gaussian beams, Gaussian packets are, at any given time, concentrated close to the central point of the packet. Thus, we can consider only those packets, which fall into the target zone.

Moreover, we can pick out Gaussian packets contributing to the target zone, multiply their amplitudes by corresponding weighting factors, and use them in the recomposition of the common-shot gather. In such a case, we obtain the wave field scattered specifically from the target zone.

6 Numerical examples

We tested our method on the Marmousi data set (Versteeg & Grau, 1991). The Marmousi model represents a very complex structure, see Figure 1. The dimensions of the model are 9200 metres (length) by 3000 metres (depth). The values of velocity, which are defined on a grid of cells of 4×4 metres, vary from 1500 ms^{-1} to 5500 ms^{-1}. Since the original model is not suitable for any ray method, we minimized the relevant Sobolev norm of slowness as described in Section 4.1, and obtained three different smooth velocity models, see Figure 2. Each model is characterized by its *average Lyapunov exponent* λ (Klimeš, 2002; Žáček, 2002), which controls the average geometrical spreading of the ray field. The average Lyapunov exponent reads $\lambda = 0.52\ \mathrm{s}^{-1}$ for the model in Figure 2a, $\lambda = 0.68\ \mathrm{s}^{-1}$ for the model in Figure 2b, and $\lambda = 0.89\ \mathrm{s}^{-1}$ for the model in Figure 2c.

The Gaussian packet migration operates in the common-shot domain. Following the procedure explained in Section 4.3, we decompose the common-shot gather, see Figure 3a, into individual Gabor functions, see Figure 3b. The complex-valued amplitude of a Gaussian packet equals the amplitude of the corresponding Gabor function. Using expression (62), we calculate the localized image of a single Gabor function from the

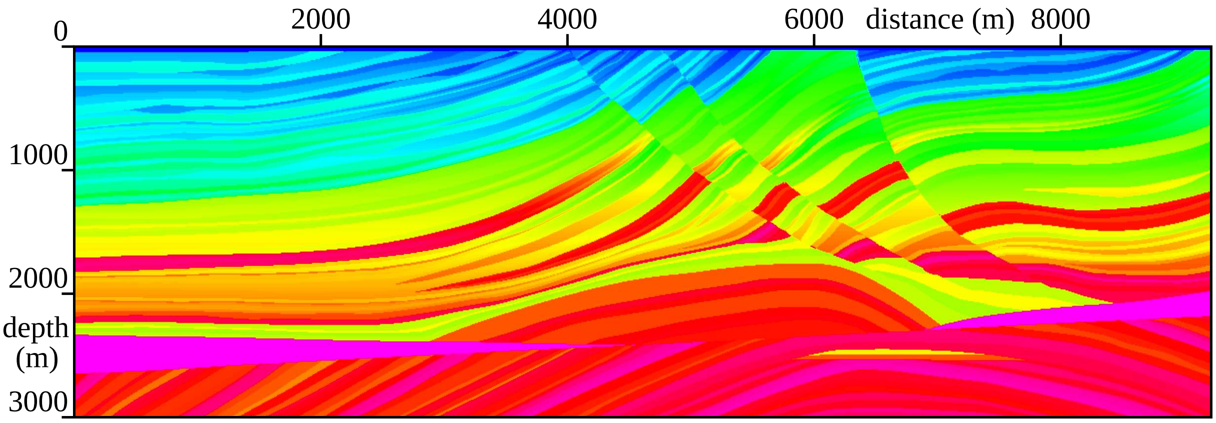

Figure 1. Marmousi model (Versteeg & Grau, 1991).

common-shot gather, see Figure 3c. Let us point out that Figures 3b and 3c demonstrate the unique one-to-one relation between the Gabor function from the common-shot gather and its localized image from the migrated section. Finally, we superimpose all relevant images according to relation (65), and obtain the prestack migrated image of the common-shot gather, see Figure 3d.

In Figure 4, we present the migrated images of individual Gabor functions for three different arrival times of a Gaussian packet t_{R}, but for the same coordinate of the intersection of the central ray of a Gaussian packet with the profile x_{R}, the same component of the slowness vector along the profile p, and the same frequency ω.

In Figure 5, we show the migrated images of individual Gabor functions for three different frequencies ω, but for the same coordinate of the intersection of the central ray of a Gaussian packet with the profile x_{R}, the same arrival time t_{R}, and the same component of the slowness vector along the profile p.

Summation of the migrated images of Gabor functions of a fixed shape over all arrival times t_{R} yields the migrated image of a corresponding Gaussian beam. In Figure 6, we demonstrate such summation for three different frequencies ω, but for the same coordinate of the intersection of the central ray with the profile x_{R} and the same component of the slowness vector along the profile p. Please note that the colour coded amplitudes in Figures 3, 4, 5 and 6 are normalized and do not represent the true amplitudes.

Since we wish to minimize the spreading, we optimize the initial shape of Gaussian packets according to the procedure suggested in Section 4.2. To simplify the tests, we have decided to smooth the resulting distribution of parameter N^0 on the Hamiltonian hypersurface in the phase-space to a constant value. Such smoothing is sensitive to the maximum travel time we take into account. Moreover, the smoothed uniform parameters of Gaussian packets vary for different common-shot gathers. As not all the common-shot gathers are equally important for the optimization, we cannot simply average corresponding parameters N^0 with uniform weights. Therefore, the choice of the most suitable parameter N^0 for the whole data set depends not only on the strict mathematical procedure suggested by Žáček (2001a, 2001b), but also on our experience. We select $\mathrm{Re}(N^0) = -0.25 \times 10^{-6}$ sm^{-2} and $\mathrm{Im}(N^0) = 0.25 \times 10^{-6}$ sm^{-2}. Parameter K^0, which describes the shape of a Gaussian packet along the central ray, is considered pure imaginary, $\mathrm{Im}(K^0) = 8.8$ s^{-2}.

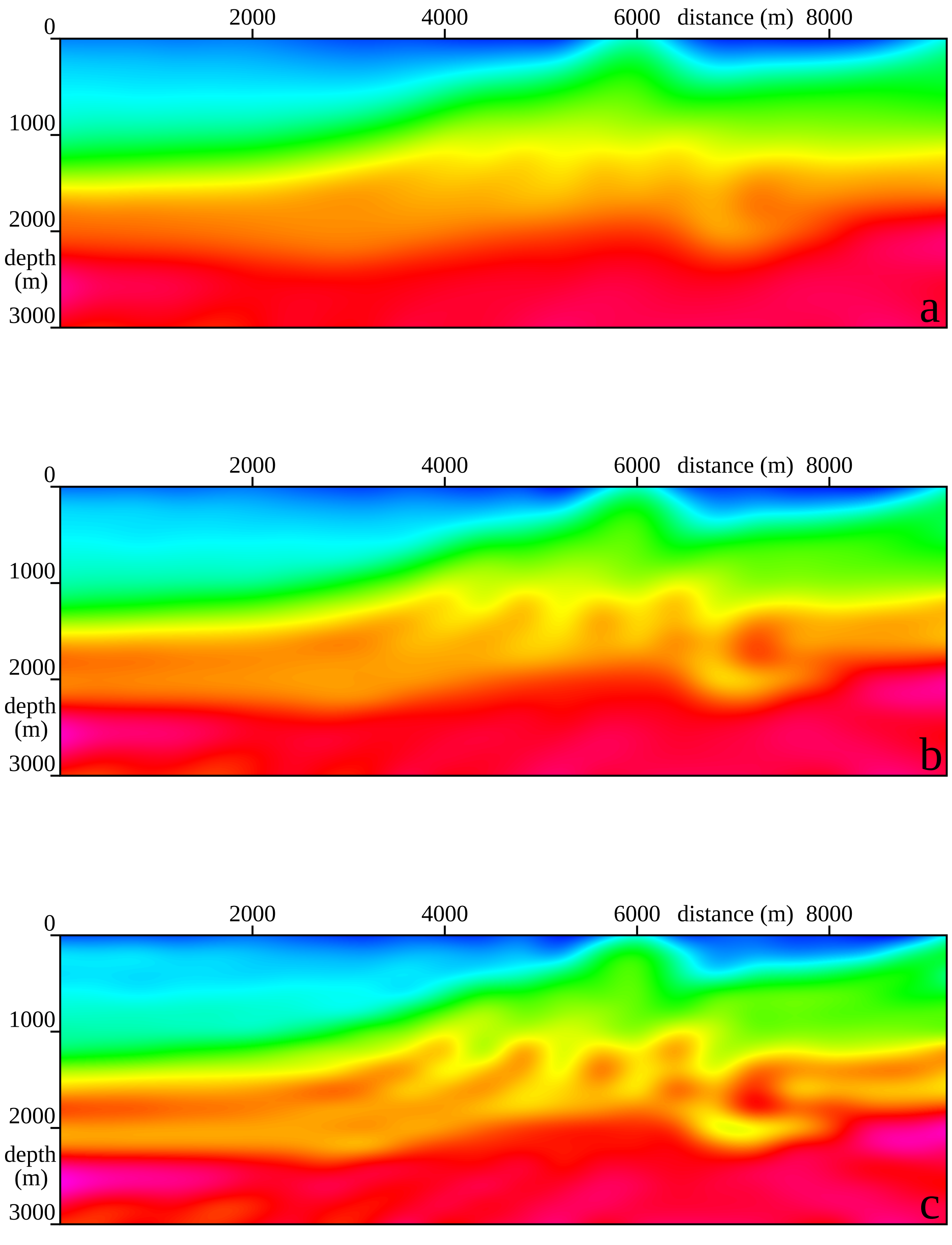

Figure 2. Smoothed models with the average Lyapunov exponents λ of (a) 0.52 s^{-1}, (b) 0.68 s^{-1} and (c) 0.89 s^{-1}. The average Lyapunov exponent controls the average geometrical spreading of the ray field.

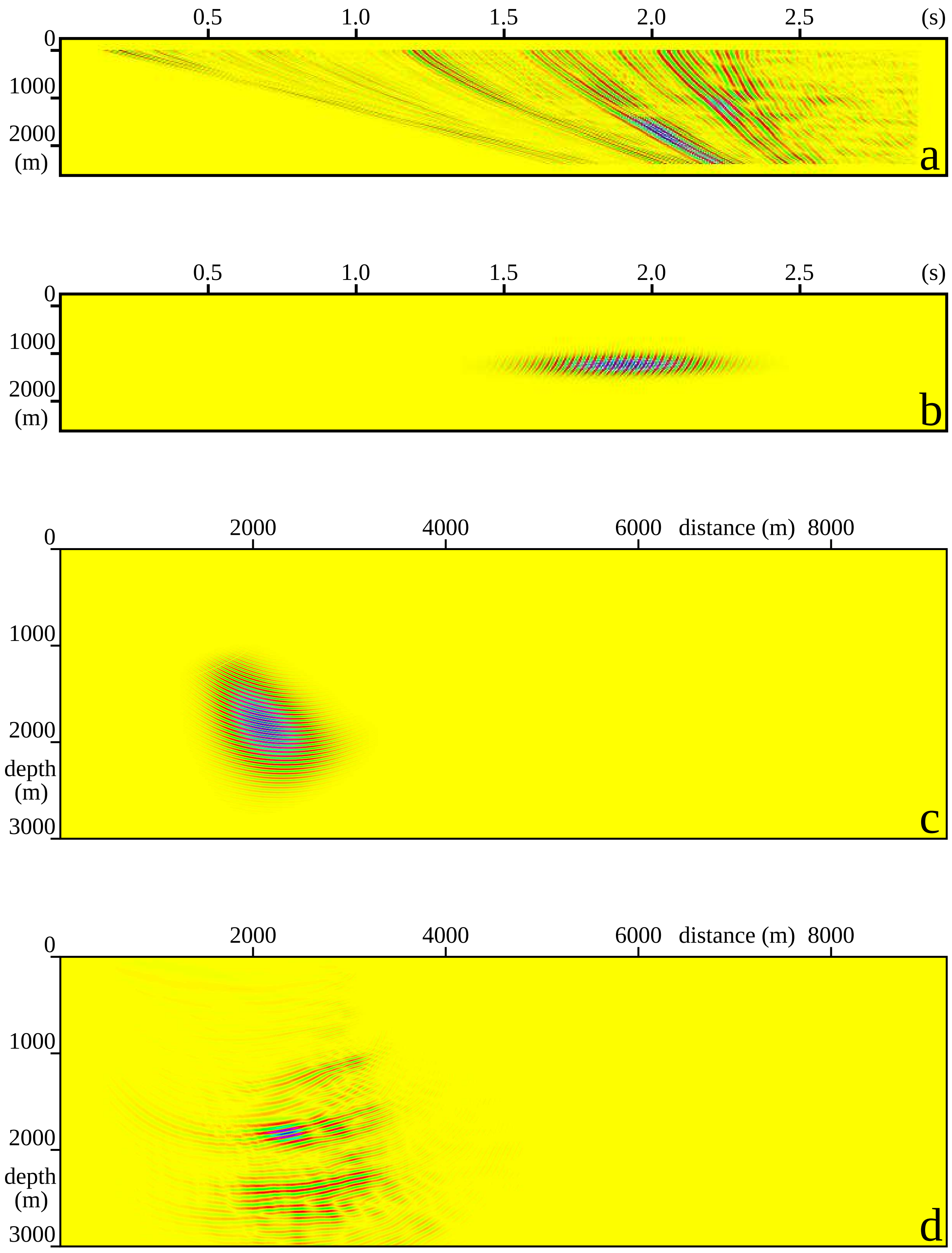

Figure 3. We decompose the common-shot gather of the Marmousi data set (a) into individual Gabor functions (b). Each Gabor function generates its localized image in the depth section (c). Superimposing all relevant images, we obtain the migrated image of the common-shot gather (d).

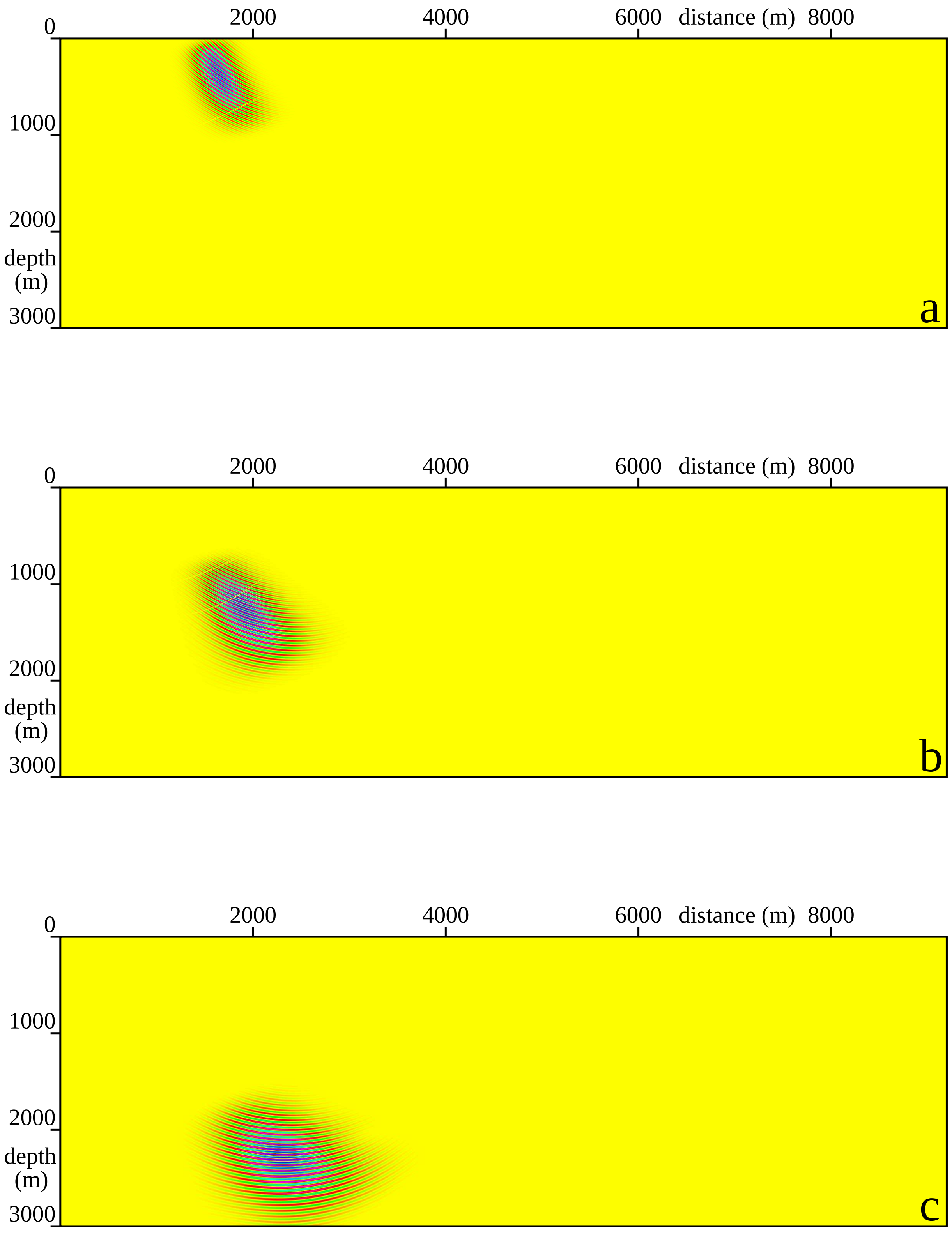

Figure 4. Migrated images of individual Gabor functions for three different arrival times t_{R}, but for the same coordinate of the intersection of the central ray of a Gaussian packet with the profile x_{R}, the same component of the slowness vector along the profile p, and the same frequency ω.

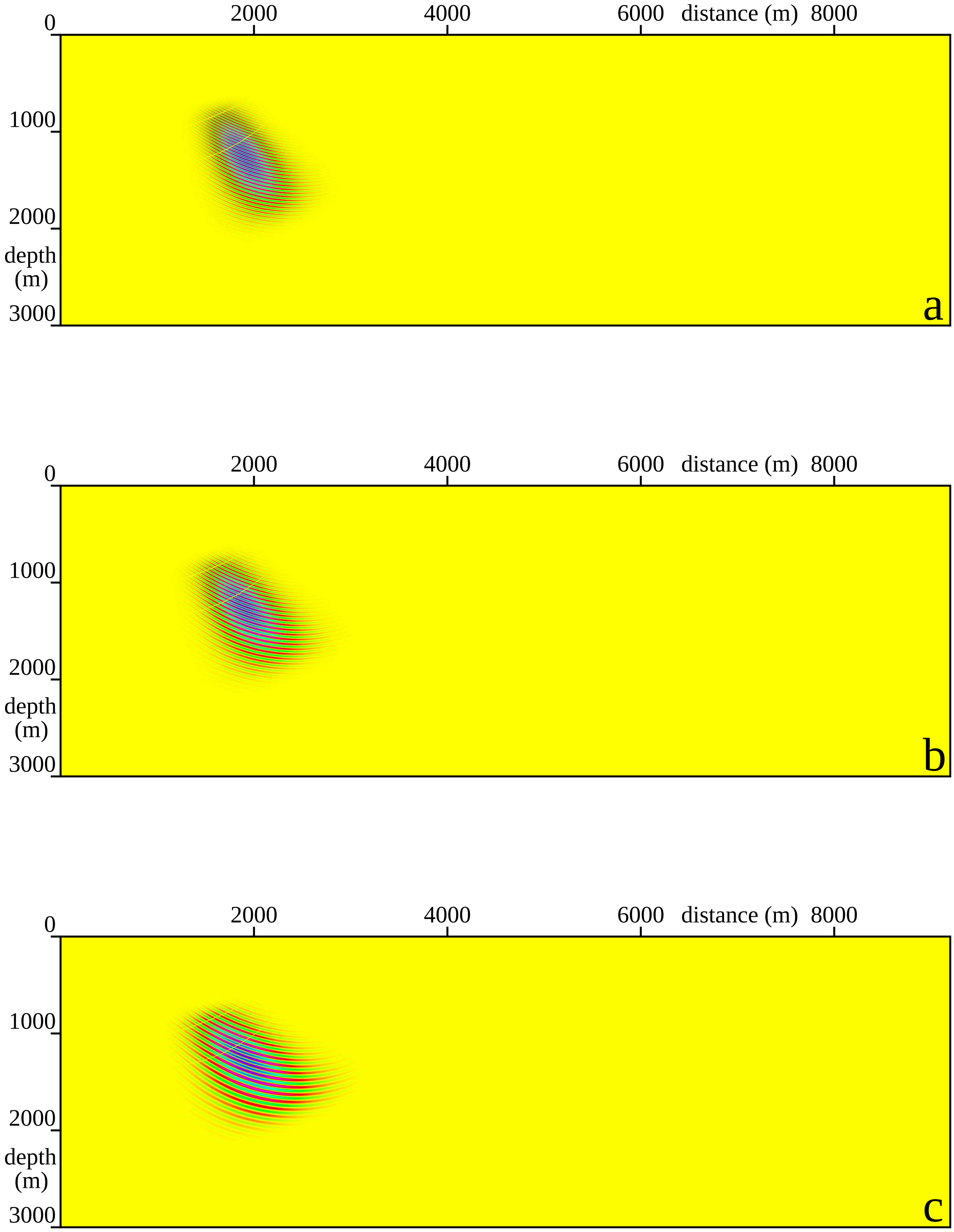

Figure 5. Migrated images of individual Gabor functions for three different frequencies ω, but for the same coordinate of the intersection of the central ray of a Gaussian packet with the profile x_{R}, the same arrival time t_{R}, and the same component of the slowness vector along the profile p.

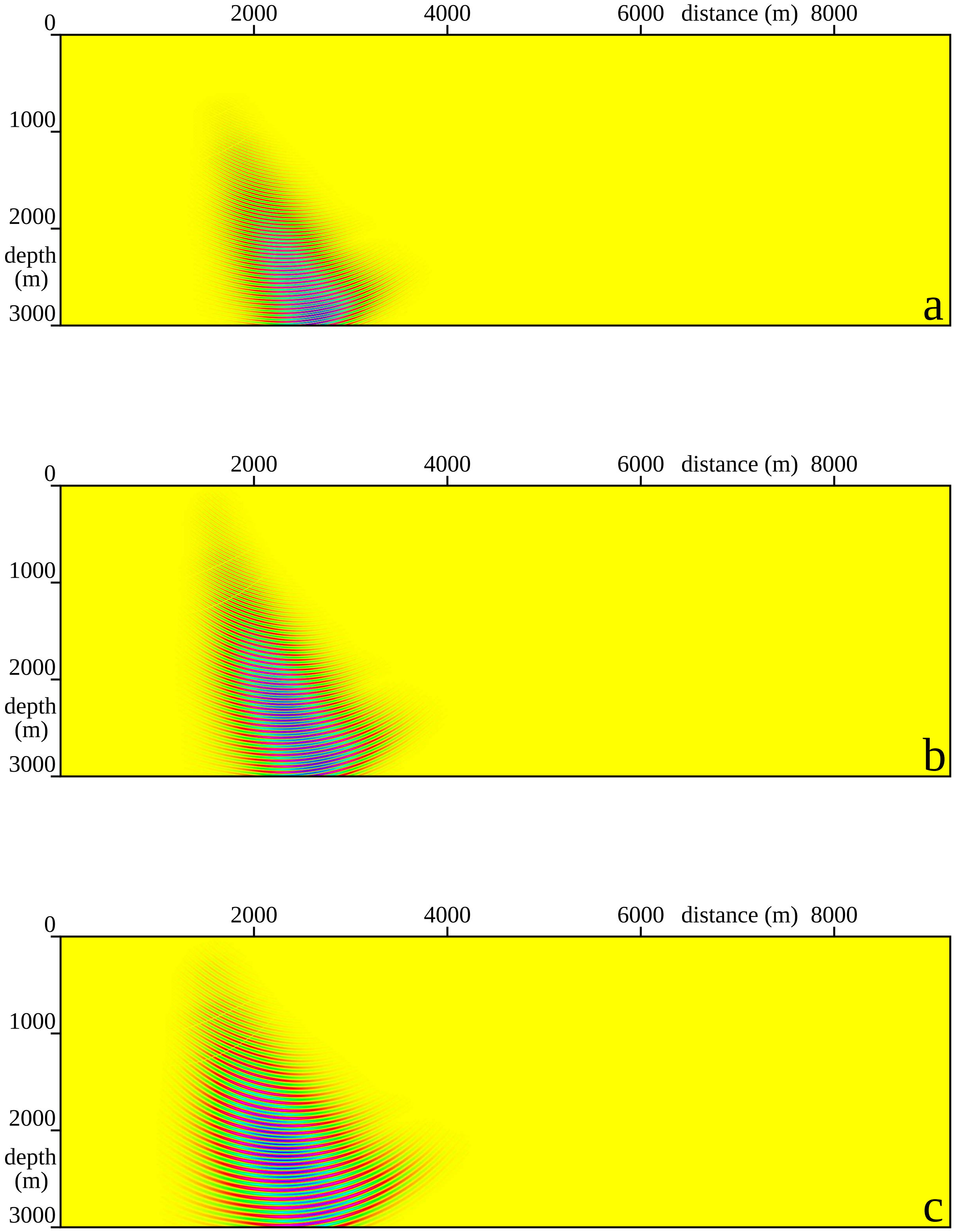

Figure 6. Migrated images of Gabor functions summed over all arrival times t_R for three different frequencies ω, but for the same coordinate of the intersection of the central ray of a Gaussian packet with the profile x_R and the same component of the slowness vector along the profile p. These images correspond to migrated images of Gaussian beams.

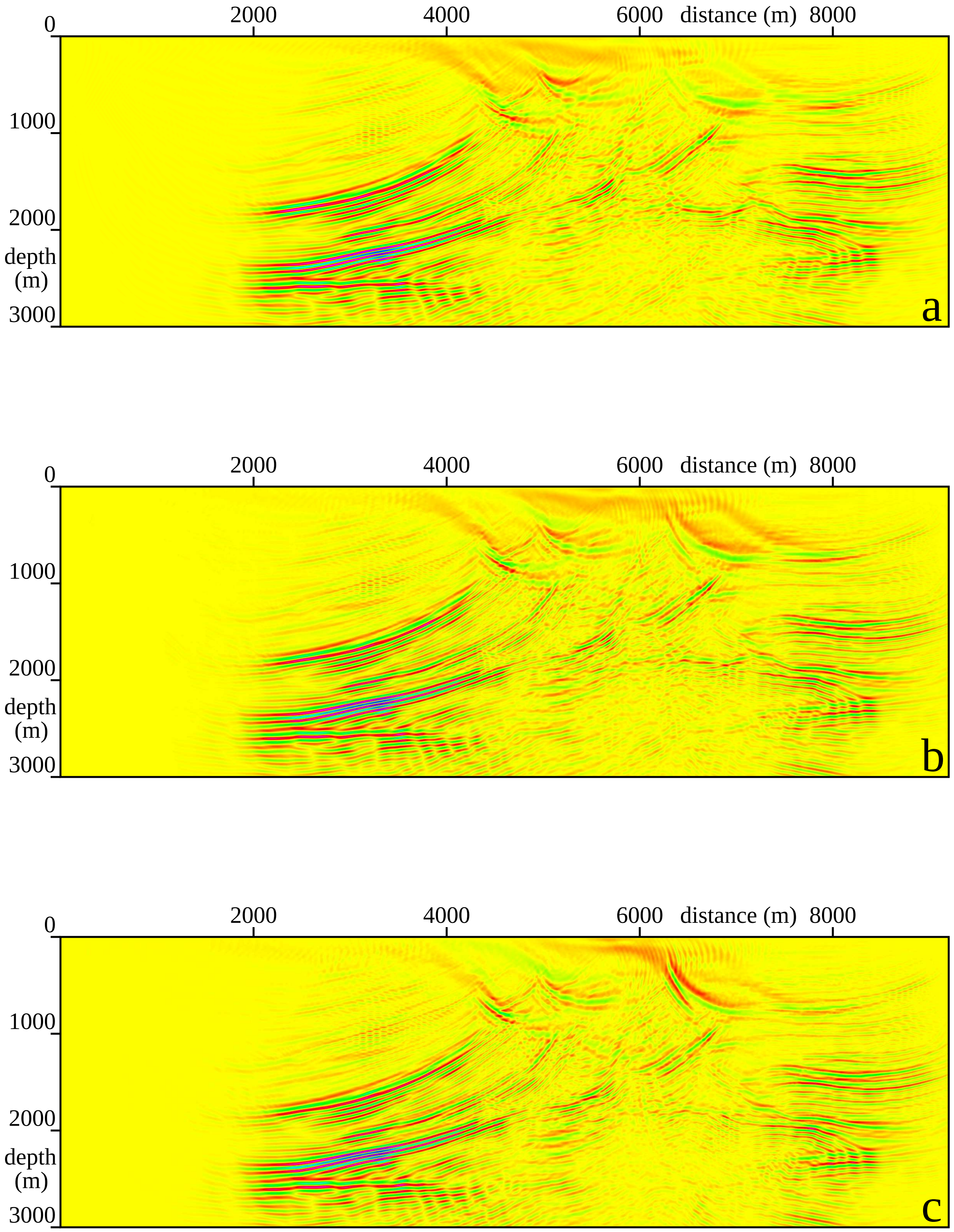

Figure 7. Stacked migrated sections of the Marmousi data set calculated in the velocity models with the average Lyapunov exponents λ of (a) 0.52 s^{-1}, see Figure 2a, (b) 0.68 s^{-1}, see Figure 2b, and (c) 0.89 s^{-1}, see Figure 2c. We used a sparse grid of cells of 20×20 metres and applied no post-processing.

A proper choice of the discretization of the phase-space is of key importance in the decomposition of the wave field into Gaussian packets. Using the method proposed by Žáček (2003, 2005), we obtain $\Delta x_{\mathrm{R}} = 82.1$ m, $\Delta t_{\mathrm{R}} = 0.272$ s, $\Delta p = 0.404 \times 10^{-4}$ sm^{-1} and $\Delta\omega = 3.70$ s^{-1}. We decomposed the original Marmousi data and did not apply any pre-processing.

The stacked migrated sections of the Marmousi data set are displayed in Figure 7. They correspond to three different smooth models, see Figure 2, and represent the raw output of our method. In order to speed the calculation up, we used a sparser grid of cells of 20×20 metres.

Although we can recognize several features of the Marmousi model, we failed in reconstructing the bottom part of the model. We believe three main causes of such result consist in (a) the use of *uniform* Gaussian packets, (b) oversimplified stacking procedure, and (c) considerably smoothed velocity models, see Versteeg (1993). Nevertheless, we are still intensively testing our method, and therefore the numerical examples shown in Figure 7 should be considered as very preliminary.

In the future, we would like to refine the method of stacking in order to improve the quality of stacked migrated sections. Moreover, we should consider the application of Gaussian packets with varying parameter N^0. This would make the Gaussian packet prestack depth migration more expensive, but also more suitable for complex velocity models.

7 Conclusions

The Gaussian packet prestack depth migration represents a new and promising imaging method operating in the common-shot domain. It can handle multi-valued travel times and allows a target-oriented approach.

Although the common-shot Gaussian packet migration cannot match the efficiency of the common-offset Gaussian beam migration algorithm proposed by Hill (2001), it is more general and provides a one-to-one relation between the Gabor functions from the common-shot gather and their localized images from the depth section. We hope that this unique feature could help us in understanding the true meaning of the migrated section.

Ultimately, we would like to inspire and encourage other researchers and possibly attract their attention to the Gaussian packet domain. We believe that it could show even greater potential than the well-known Gaussian beam domain.

Acknowledgements

The author is greatly indebted to Luděk Klimeš for guidance throughout the work on this topic.

The research has been supported by the Grant Agency of the Czech Republic under Contract 205/04/1104, by the Grant Agency of the Charles University under Contract 375/2004/B-GEO/MFF, and by the members of the consortium "Seismic Waves in Complex 3-D Structures" (see "http://sw3d.mff.cuni.cz").

References

Babich, V. M. & Ulin, V. V. (1981): Complex space time ray method and 'quasiphotons'. Zap. Nauchn. Sem. Leningr. Otd. Math. Inst., **117**, 5–12 (in Russian); English transl.: J.Sov. Math., **24**, 269–273, 1984.

Bulant, P. & Klimeš, L. (1999): Interpolation of ray-theory travel times within ray cells. Geophys. J. Int., **139**, 273–282.

Červený, V. (2001): Seismic Ray Theory. Cambridge Univ. Press, Cambridge.

Hill, N. R. (1990): Gaussian beam migration. Geophysics, **55**, 1416–1428.

Hill, N. R. (2001): Prestack Gaussian-beam depth migration. Geophysics, **66**, 1240–1250.

Klimeš, L. (1989a): Gaussian packets in the computation of seismic wavefields. Geophys. J. Int., **99**, 421–433.

Klimeš, L. (1989b): Optimization of the shape of Gaussian beams of a fixed length. Stud. geophys. geod., **33**, 146–163.

Klimeš, L. (2002): Lyapunov exponents for 2-D ray tracing without interfaces. Pure and Appl. Geophys., **159**, 1465–1485.

Klimeš, L. (2004): Gaussian packets in smooth isotropic media. In: Seismic Waves in Complex 3-D Structures, Report 14, Charles University, Prague, 43–54.

Ralston, J. (1983): Gaussian beams and the propagation of singularities. MAA Studies in Mathematicc., **23**, 206–248.

Versteeg, R. J. & Grau, G. (eds.) (1991): The Marmousi experience. Proc. EAGE workshop on Practical Aspects of Seismic Data Inversion (Copenhagen, 1990), Eur. Assoc. Explor. Geophysicists, Zeist.

Versteeg, R. J. (1993): Sensitivity of prestack depth migration to the velocity model. Geophysics, **58**, 873–882.

Žáček, K. (2001a): Optimization of the shape of Gaussian beams. 71st Ann. Int. Mtg., Soc. Expl. Geophys., Expanded Abstracts, 2128–2131.

Žáček, K. (2001b): Optimization of the shape of Gaussian beams. In: Seismic Waves in Complex 3-D Structures, Report 11, Charles University, Prague, 181–201.

Žáček, K. (2002): Smoothing the Marmousi model. Pure and Appl. Geophys., **159**, 1507–1526.

Žáček, K. (2003): Decomposition of the wave field into optimized Gaussian packets. 73st Ann. Int. Mtg., Soc. Expl. Geophys., Expanded Abstracts, 1869–1872.

Žáček, K. & Klimeš, L. (2003): Sensitivity of seismic waves to the structure. 73rd Ann. Int. Mtg., Soc. Expl. Geophys., Expanded Abstracts, 1857–1860.

Žáček, K. (2004): Gaussian packet pre-stack depth migration. 74th Ann. Int. Mtg., Soc. Expl. Geophys., Expanded Abstracts, 957–960.

Žáček, K. (2005): Decomposition of the wave field into optimized Gaussian packets. In: Seismic Waves in Complex 3-D Structures, Report 15, Charles University, Prague.